On the optimised magnetic dynamo

Ashley P. Willis
School of Mathematics and Statistics, University of Sheffield, S11 7RH, U.K.
(Dated: September 7, 2012)

In stars and planets, magnetic fields are believed to originate from the motion of electrically conducting fluids in their interior, through a process known as the dynamo mechanism. In this letter, optimisation of the velocity field for magnetic energy growth enables us to simultaneously address two fundamental questions of dynamo theory: "Which velocity field leads to the most magnetic energy growth?" and "How large does the velocity need to be relative to magnetic diffusion?". Here the full space of continuous solenoidal velocity fields in a periodic box is considered. Measuring the strength of the flow with the root-mean-square amplitude, an optimal velocity field is shown to exist, but without limitation on the strain rate, it is locally optimal only. Measuring the flow in terms of its associated dissipation leads to the identification of a single optimal at the critical magnetic Reynolds number necessary for a dynamo. This is found to be only 15% higher than that necessary for transient growth of the magnetic field, implying that stationary velocity fields are sufficient at low magnetic Reynolds number.

PACS numbers: 47.20.-k,95.30.Qd,47.54.-r

The continuous stretching and folding of magnetic field lines by a velocity field is considered to be the main mechanism generating magnetic fields in stars, planets and the interstellar media [1]. This magnetic dynamo mechanism must counter magnetic diffusion, which occurs on a time scale that can be estimated by L^2/λ, where L is the length scale of the system and λ is the magnetic diffusivity. Together with a scale for the velocity U, the relative growth versus diffusion can be estimated with the magnetic Reynolds number, $Rm = LU/\lambda$. Without complete knowledge of the interior flows of astrophysical bodies, theoretical studies have considered many parametrised velocity fields in several geometries, including the Ponomorenko [2], Roberts [3], ABC [4, 5] and Dudley and James flows [6], over the last 40 years. Systematic searches continue to seek the best dynamo possible dynamos within the parameter space, e.g. [7].

The small length scale of the laboratory compared to astrophysical bodies implies rapid diffusion, and the mechanism is therefore difficult to reproduce. Nevertheless, this is an exciting era where laboratory experiments have begun to realise this process [8–10]. The experiments vary greatly in geometry, but in order to be successful, all seek to optimise the flow conditions necessary to realise magnetic energy growth.

In this letter, optimisation is shown to be possible without need for the specification of a parametrised set of acceptable flows. This enables a lower bound on the magnetic Reynolds number to be identified for a dynamo. Optimising for both long- and short-term growth reveals that the dynamo mechanism need not rely on transient growth effects to work well, and that a stationary velocity field is sufficient at low Rm.

Throughout this letter, the length scale is taken to be $L = L_x/(2\pi)$, so that the scaled box has length 2π in each direction, and the following notations are used:

$$\boldsymbol{v}^2 = \boldsymbol{v}\cdot\boldsymbol{v}, \quad \langle a\rangle = \frac{1}{V}\int a\,\mathrm{d}V, \quad ||a||_2 = \langle a^2\rangle^{\frac{1}{2}}, \qquad (1)$$

where V is the volume of the box, so that $||\cdot||_2$ is equivalent to the root-mean-square value. To begin with, the velocity scale is taken to be $U = ||\boldsymbol{u}||_2$.

A variational optimisation method is used to find the velocity field $\boldsymbol{u}$ that maximises the growth in $\boldsymbol{B}$ after a period of time T. This method has recently proven useful in the study of the growth of disturbances in shear flows [11, 12]. Consider the objective function

$$\begin{aligned}\mathcal{L} = {} & \langle \boldsymbol{B}_T^2\rangle \;-\; \lambda_1\,(\langle \boldsymbol{u}^2\rangle - 1) \;-\; \lambda_2\,(\langle \boldsymbol{B}_0^2\rangle - 1) \\ & -\langle \Pi_1\,\boldsymbol{\nabla}\cdot\boldsymbol{u}\rangle - \langle \Pi_2\,\boldsymbol{\nabla}\cdot\boldsymbol{B}_0\rangle \qquad (2)\\ & -\int_0^T \langle \boldsymbol{\Gamma}\cdot[\partial_t\boldsymbol{B} - \boldsymbol{\nabla}\times(\boldsymbol{u}\times\boldsymbol{B}) - \frac{1}{Rm}\boldsymbol{\nabla}^2\boldsymbol{B}]\,\rangle \mathrm{d}t\,.\end{aligned}$$

The first term on the right-hand side is to be maximised. The remaining terms are constraints, including Lagrange multipliers λ_i, $\Pi_i = \Pi_i(\boldsymbol{x})$ and $\boldsymbol{\Gamma} = \boldsymbol{\Gamma}(\boldsymbol{x})$. These terms are enforced to be zero. After applying variational derivatives it may be written that

$$\begin{aligned}\delta\mathcal{L} = {} & \langle \frac{\delta\mathcal{L}}{\boldsymbol{\delta u}}\cdot\boldsymbol{\delta u}\rangle + \langle \frac{\delta\mathcal{L}}{\boldsymbol{\delta B}_0}\cdot\boldsymbol{\delta B}_0\rangle + \langle \frac{\delta\mathcal{L}}{\boldsymbol{\delta B}_T}\cdot\boldsymbol{\delta B}_T\rangle \\ & -\int_0^T \langle \boldsymbol{\delta\Gamma}\cdot[\mathrm{ind.}]\,\rangle \mathrm{d}t - \int_0^T \langle \boldsymbol{\delta B}\cdot[\mathrm{adj.}]\,\rangle \mathrm{d}t\,, \qquad (3)\end{aligned}$$

where

$$\frac{\delta\mathcal{L}}{\boldsymbol{\delta u}} = \int_0^T \boldsymbol{B}\times(\boldsymbol{\nabla}\times\boldsymbol{\Gamma})\,\mathrm{d}t - 2\,\lambda_1\,\boldsymbol{u} + \boldsymbol{\nabla}\Pi_1, \qquad (4)$$

$$\frac{\delta\mathcal{L}}{\boldsymbol{\delta B}_0} = \boldsymbol{\Gamma}_0 - 2\,\lambda_2\,\boldsymbol{B}_0 + \boldsymbol{\nabla}\Pi_2, \qquad (5)$$

$$\frac{\delta\mathcal{L}}{\boldsymbol{\delta B}_T} = 2\,\boldsymbol{B}_T - \boldsymbol{\Gamma}_T, \qquad (6)$$

"ind." represents the induction equation, as it appears in (2), and "adj." is set to zero giving the adjoint equation

$$-\,\partial_t \mathbf{\Gamma} = (\boldsymbol{\nabla}\times\mathbf{\Gamma})\times\boldsymbol{u} + \frac{1}{Rm}\boldsymbol{\nabla}^2\mathbf{\Gamma}\,. \tag{7}$$

In deriving these expressions it is necessary to lift derivatives off the variations, for example

$$\begin{aligned}\langle \Pi\,\boldsymbol{\nabla}\cdot\boldsymbol{\delta v}\rangle &= \langle \Pi\,\partial_i\,\delta v_i\rangle = \langle \partial_i\Pi\,\delta v_i\rangle - \langle \delta v_i\,\partial_i\Pi\rangle \\ &= \frac{1}{V}\int \Pi\,\boldsymbol{\delta v}\cdot\mathbf{d}\boldsymbol{S} - \langle \boldsymbol{\delta v}\cdot\boldsymbol{\nabla}\Pi\rangle,\end{aligned} \tag{8}$$

where the product rule and Gauss' Theorem have been used. For the first of the final two terms, the integral over the closed surface vanishes for case of the periodic box. For the second, it is quite beautiful that the Lagrange multipliers themselves provide projection functions — these will be used to ensure that $\boldsymbol{u}$ and $\boldsymbol{B}_0$ are solenoidal.

For a given $\boldsymbol{u}$ and $\boldsymbol{B}_0$, both solenoidal and normalised, timestepping the induction equation to give $\boldsymbol{B}_T$ ensures that the penultimate term on the right-hand side of (3) is zero. Then $\partial\mathcal{L}/\boldsymbol{\delta B}_0$ in (3) and (6) is set to zero with the compatibility condition $\mathbf{\Gamma}_T = 2\,\boldsymbol{B}_T$. Given $\mathbf{\Gamma}_T$, timestepping the adjoint backwards sets the last term in (3) to zero and provides $\mathbf{\Gamma}_0$. Now all quantities are known to calculate ascent directions for $\mathcal{L}$ given by (4) and (5). New fields that lead to an increased $\mathcal{L}$ are given by $\boldsymbol{u} := \boldsymbol{u}+\epsilon\,(\delta\mathcal{L}/\boldsymbol{\delta u})$ and $\boldsymbol{B}_0 := \boldsymbol{B}_0+\epsilon\,(\delta\mathcal{L}/\boldsymbol{\delta B}_0)$, where ϵ is a small scalar value. The new fields are projected onto the space of solenoidal functions by considering the divergence of the update, which defines the projections functions Π_i. After this, the λ_i are then chosen such that the new fields have unit norm, and all constraint terms in (2) are then zero.

The value of ϵ is adjusted according to whether or not consecutive updates appear to be pointing in a similar direction. Note also that $\boldsymbol{B}$ needs to be known for all intermediate times during the backwards integration of $\mathbf{\Gamma}$. This could require significant computer memory. Instead $\boldsymbol{B}$ may be saved at 'checkpoints' and re-integrated forwards when need, involving only 50% extra work overall. Spatial discretisation used in the time-stepping code is via a triple-Fourier expansion. Nonlinear terms are evaluated pseudospectrally on a grid with at least 36 points in each direction. This resolution was found to be more than sufficient for the majority of calculations, where Rm is very low.

Figure 1 shows the result of calculations starting from several random initial $\boldsymbol{u}$ and $\boldsymbol{B}_0$ at $Rm = 1$. All converge to the same optimal, and the error, measured by $(\langle(\delta\mathcal{L}/\boldsymbol{\delta u})^2\rangle + \langle(\delta\mathcal{L}/\boldsymbol{\delta B}_0)^2\rangle)^{\frac{1}{2}}$ drops by 5 orders of magnitude during the calculation. A sure test that the end state is an optimal is to verify that perturbations lead to a decrease in the growth. The sensitivity to perturbations of the optimal is shown in the inset to Figure 1, where the growth rate σ of the field $\boldsymbol{B}$ is estimated at

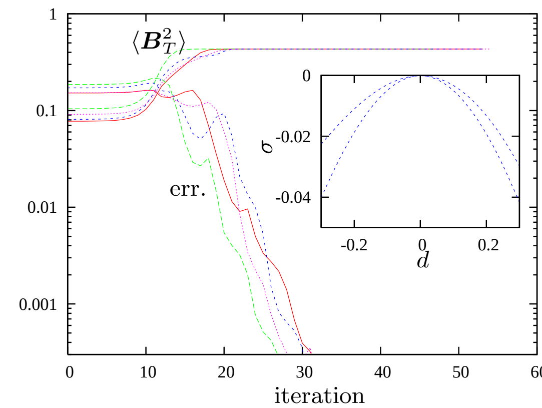

FIG. 1. Several initial conditions converge to the same optimal; $Rm = 1$, $T = 1$. *Inset*: Sensitivity of the optimal $\boldsymbol{u}_{op}$ at $Rm = 1.737$ to perturbations $\boldsymbol{u}_p$ measured by the growth rate, σ in units $||u||_2/L$. Here $\boldsymbol{u} = \alpha(\boldsymbol{u}_{op} + d\,\boldsymbol{u}_p)$ and all velocity fields have unit norm.

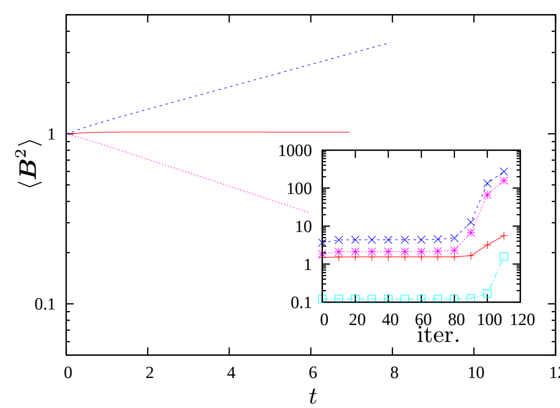

FIG. 2. Magnetic energy for converged optima at $Rm = 1.5$, 1.737 and 2.0. By time T the signal is dominated by the leading eigenmode. *Inset*: Divergence for $Rm = 2.2$; quantities from bottom to top are σ, $||S||_2 = ||\boldsymbol{\omega}||_2$, $||\boldsymbol{\omega}||_\infty$ and $||S||_\infty$,

time $T = 7$. At this low Rm the optimal is apparently quite robust.

Increasing Rm, the optimal $\boldsymbol{u}_{op}$ is found to change little until at $Rm = 1.737$ the growth rate σ is zero. Figure 2 shows the dependence of $\langle\boldsymbol{B}^2\rangle$ with time. At these low Rm only modest transient growth is observed. By time T the energy is steady and $\boldsymbol{B}_T$ is dominated by the leading eigenmode. In this non-dimensionalisation the diffusion time L^2/λ is equal to $t = Rm$ in units $L/||\boldsymbol{u}||_2$. Helicity is plotted in Figure 3 to give a sense of the geometry and symmetry of the flow. The magnetic field, however, is concentrated at a subset of the stagnation points in the flow; see [13] for plots where the dynamo mechanism appears to be similar.

Although the optimal can be traced a little beyond $Rm = 2$, it becomes clear that its basin of optimality rapidly becomes vanishingly small, as not all op-

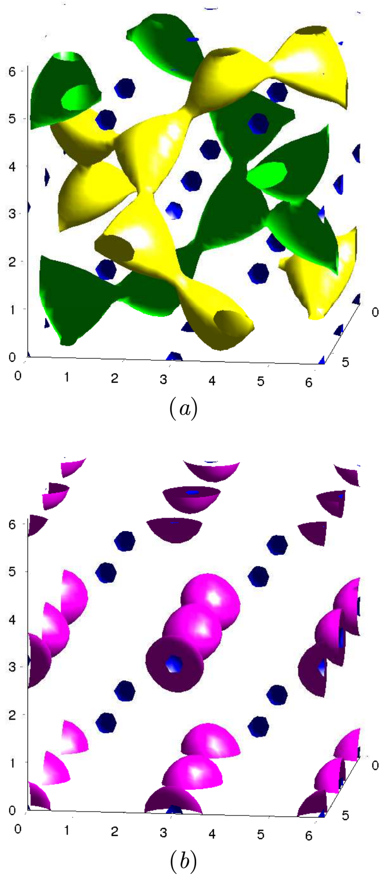

FIG. 3. Optimal at $Rm = 1.737$. (a) Isosurfaces of positive and negative helicity $\boldsymbol{u}\cdot\boldsymbol{\omega}$ (yellow, green) and stagnation points (blue). (b) Isosurfaces of $\boldsymbol{B}_T^2$ (pink).

timisations converge. While the scaled velocity satisfies $||\boldsymbol{u}||_2 = 1$, the strain rate $S = (2\,S_{ij}\,S_{ij})^{\frac{1}{2}}$, where $S_{ij} = \frac{1}{2}(\partial_i\,u_j + \partial_j\,u_i)$, is unlimited. Large S is known to lead to large growth. The inset to Figure 2 shows an example where the method deviates from the local optimal at $Rm = 2.2$. Improved resolution does not remedy the problem, it only permits even finer structures to form.

A more appropriate measure of the flow is therefore necessary, here taken to be the velocity scale $U = L\,||S||_2$. Whilst S and the vorticity $\omega = |\boldsymbol{\omega}|$ are not equal locally, it can be shown that $||S||_2 = ||\omega||_2$. The latter is somewhat more convenient to work with in the variational method. The scaled velocity field satisfies $||\boldsymbol{\omega}||_2 = 1$, so that optimisation can be considered to be over the space of fields with equal viscous dissipation or input power driving the flow, neglecting any feedback on the flow from the magnetic field. This scaling leads to the magnetic Reynolds number

$$Rm_\omega = \frac{L^2\,||\omega||_2}{\lambda}. \tag{9}$$

In a similar context, Backus [14] derived a lower limit for dynamos in a sphere in terms of the analogous magnetic Reynolds number except involving $||S||_\infty$ rather than $||S||_2$. Although not used further here, higher norms of S and ω are observed to behave similarly; see the inset to Figure 2.

The optimisation is only slightly altered, where now

$$\mathcal{L} = \langle \boldsymbol{B}_T^2 \rangle \;-\; \lambda_1(\langle \boldsymbol{\omega}^2 \rangle - 1) \;-\; \ldots \tag{10}$$

and the new update is given by

$$\frac{\delta\mathcal{L}}{\boldsymbol{\delta u}} \;=\int_0^T \boldsymbol{B}\times(\boldsymbol{\nabla}\times\boldsymbol{\Gamma})\,\mathrm{d}t - 2\lambda_1\,\boldsymbol{\nabla}\times\boldsymbol{\omega} + \boldsymbol{\nabla}\Pi_1. \tag{11}$$

Similar to before, the scalar λ_1 is chosen such that for the new $\boldsymbol{u}$ one has $\langle \boldsymbol{\omega}^2 \rangle = 1$. The extra complexity of the update leads to a linear approximation that is valid over a shorter range, and the number of iterations necessary for convergence is typically order 1000, compared with order 100 before.

Upon optimisation with the vorticity scaling, almost the same optimal was found at $Rm_{\omega c} = 2.48$. Its corresponding $Rm = 1.75$, now an observed quantity, is only slightly higher than found previously, where is was optimised for Rm. Starting from 20 initial conditions at $Rm_{\omega c}$, all converged to the same optimal. Figure 4 compares growth rates for the optimal found at $Rm = 1.737$, where $\boldsymbol{u}$ is fixed and Rm_ω is varied, with the optimal that could now be tracked up to $Rm_\omega = 100$. For this range of Rm_ω the fixed velocity field is competitive with the optimised state, which changes relatively little. From $Rm_\omega = 2.48$ to 100 it remains an optimal with only a relative change of 8%. The inset shows that the optimal remains fairly robust to perturbations. Beyond $Rm_\omega = 100$, convergence was found to be possible using a higher norm $||\omega||_4$, but this incurs further iterations for convergence. Optimisation at higher Rm becomes computationally expensive — in addition to increased spatial resolution and more iterations, larger target times T are necessary to pass longer transients.

Time dependence of the velocity field is an important factor that could affect magnetic energy growth. In order for energy growth to be enhanced, the changing velocity field must exploit transient energy growth, to beat the mean of the energy growths associated with each velocity field considered separately. At low Rm, however, this affect has barely been observed. Setting T to a small value permits calculation of velocity and magnetic fields that lead to the largest initial magnetic energy growth. This is shown in Figure 5 using $T = 0.05$ and 20 initial conditions. Two optima were identified, the lowest sets the energy stability bound at $Rm_{\omega g} = 2.12$.

In summary, a minimum magnetic Reynolds number is found for a kinematic dynamo at $Rm_{\omega c} = 2.48$, by optimisation over the space of velocity fields with equal $||\omega||_2$ or associated viscous dissipation. Starting from 20 random initial conditions at this Rm_ω, it was the only

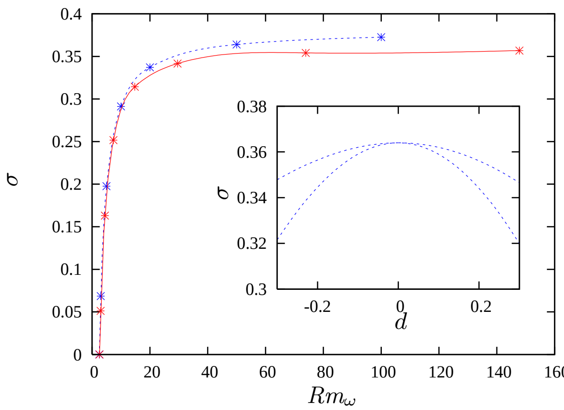

FIG. 4. Growth rates, σ in units $||\boldsymbol{\omega}||_2$, for the optimal at $Rm = 1.737$ (red, solid), where the velocity is held fixed. This is bounded above by the optimisation at each Rm_ω (blue, dashed); $Rm_{\omega c} = 2.48$. *Inset*: Growth rates for perturbations to the optimal at $Rm_\omega = 50$; disturbances as defined for Figure 1.

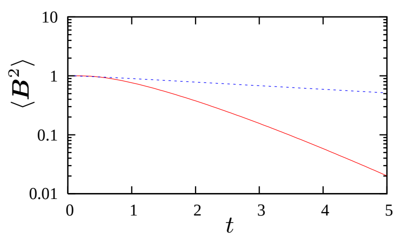

FIG. 5. Development of energy following optimised initial growth; $Rm_{\omega g} = 2.12$. The local optimal for which growth is initially zero defines $Rm_{\omega g}$ (red, solid), but it leads to rapid decay immediately following the initial 'burst'. A second optimal (blue, dashed) decays monotonically but more slowly. This second optimal is connected to that for long-term growth for $Rm_\omega \geq Rm_{\omega c}$.

optimal found. This velocity field is very close to a local optimal at $Rm = 1.737$, in the space of fields with $||\boldsymbol{u}||_2 = 1$; it is a local optimal only, as the strain rate is unlimited. A lower bound for instantaneous magnetic energy growth is found at $Rm_{\omega g} = 2.12$. This is not far below $Rm_{\omega c} = 2.48$, the lower bound found for long-term growth induced by a steady velocity field. The small difference between $Rm_{\omega g}$ and $Rm_{\omega c}$ leaves little room for improvement to be gained by time-dependent velocity fields. Transient growth will, however, be increasingly important at large Rm. While this velocity field already appears to be a fast dynamo, with a growth rate $\sigma = 0.357\,||\boldsymbol{\omega}||_2 = 0.527\,||\boldsymbol{u}||_2/L$, optimisation at larger Rm will improve this further.

As shown here, the variational method simultaneously determines a lower bound on the Reynolds number for a dynamo, whilst identifying velocity fields that maximise magnetic energy growth. It is a rare occasion that we can put a numerical figure to an important parameter. In geometries closer to experiments, tricky boundary conditions on the magnetic field for spheres and cylinders pose technical challenges, but it will be worthwhile overcoming them. It will be interesting to see if velocity fields realisable in experiment are close, or can be made closer, to optimal. That the growth rate is observed to change little for perturbations about the optimal, is promising for the dynamo's robustness. It will also be of interest to further assess the mechanism that optimises growth, and optimisation at higher Rm may identify an alternative optimals and dynamo mechanisms to that observed here.

The author thanks Eun-Jin Kim for helpful discussions and Chris Pringle for an introduction to the variational method.

[1] H. K. Moffatt, *Magnetic field generation in electrically conducting fluids* (Cambridge University Press, 1978)
[2] A. D. Gilbert, Geophysical & Astrophysical Fluid Dynamics **44**, 241 (1988)
[3] G. O. Roberts, Phil. Trans. R. Soc. Lond. A **266**, 535 (1970)
[4] V. I. Arnold, C. R. Acad. Sci. Paris **17**, 261 (1965)
[5] S. Childress, J. Math. Phys. **11**, 3063 (1970)
[6] M. Dudley and R. James, Proc. R. Soc. Lond. A **425**, 407 (1989)
[7] A. Alexakis, Phys. Rev. E **84**, 026321 (Aug 2011)
[8] A. Gailitis, O. Lielausis, E. Platacis, S. Dement'ev, A. Cifersons, G. Gerbeth, T. Gundrum, F. Stefani, M. Christen, and G. Will, Phys. Rev. Lett. **86**, 3024 (Apr 2001)
[9] R. Stieglitz and U. Müller, Phys. Fluid. **13**, 561 (2001)
[10] R. Monchaux, M. Berhanu, M. Bourgoin, M. Moulin, P. Odier, J.-F. Pinton, R. Volk, S. Fauve, N. Mordant, F. Pétrélis, A. Chiffaudel, F. Daviaud, B. Dubrulle, C. Gasquet, L. Marié, and F. Ravelet, Phys. Rev. Lett. **98**, 044502 (Jan 2007)
[11] S. Zuccher, A. Bottaro, and P. Luchini, European Journal of Mechanics - B/Fluids **25**, 1 (2006), ISSN 0997-7546
[12] C. C. T. Pringle and R. R. Kerswell, Phys. Rev. Lett. **105**, 154502 (Oct 2010)
[13] V. Archontis, S. B. F. Dorch, and Å. Nordlund, A&A **397**, 393 (2003)
[14] G. Backus, Ann. Phys. **4**, 372 (1958)